

Multi-wavelength temporal and spectral variability of the blazar OJ 287 during and after the December 2015 flare: a major accretion disc contribution

Pankaj Kushwaha^{1*}, Alok C. Gupta^{2,3†‡}, Paul J. Wiita^{4§}, Haritma Gaur²,

E. M. de Gouveia Dal Pino¹, Jai Bhagwan⁵, O. M. Kurtanidze^{6,7}, V. M. Larionov^{8,9},

G. Damljanovic¹⁰, M. Uemura¹¹, E. Semkov¹², A. Strigachev¹², R. Bachev¹², O. Vince¹⁰,

Minfeng Gu², Z. Zhang¹³, T. Abe¹¹, A. Agarwal³, G. A. Borman¹⁴, J. H. Fan¹⁵,

T. S. Grishina⁸, J. Hirochi¹¹, R. Itoh¹⁶, M. Kawabata¹¹, E. N. Kopatskaya⁸,

S. O. Kurtanidze⁶, E. G. Larionova⁸, L. V. Larionova⁸, A. Mishra³, D. A. Morozova⁸,

T. Nakaoka¹¹, M. G. Nikolashvili⁶, S. S. Savchenko⁸, Yu. V. Troitskaya⁸,

I. S. Troitsky⁸, A. A. Vasilyev⁸

¹ *Department of Astronomy (IAG-USP), University of Sao Paulo, Sao Paulo 05508-090, Brazil*

² *Key Laboratory for Research in Galaxies and Cosmology, Shanghai Astronomical Observatory, Chinese Academy of Sciences, 80 Nandan Road, Shanghai 200030, China*

³ *Aryabhata Research Institute of Observational Sciences (ARIES), Manora Peak, Nainital 263002, India*

⁴ *Department of Physics, The College of New Jersey, P.O. Box 7718, Ewing, NJ 08628-0718, USA*

⁵ *School of Studies in Physics & Astrophysics, Pt Ravishankar Shukla University, Amanaka G.E. Road, Raipur 492010, India*

⁶ *Abastumani Observatory, Mt. Kanobili, 0301 Abastumani, Georgia*

⁷ *Engelhardt Astronomical Observatory, Kazan Federal University, Tatarstan, Russia*

⁸ *Astronomical Institute, St.-Petersburg State University, 198504 St.-Petersburg, Russia*

⁹ *Pulkovo Observatory, 196140 St.-Petersburg, Russia*

¹⁰ *Astronomical Observatory, Volgina 7, 11060 Belgrade, Serbia*

¹¹ *Hiroshima Astrophysical Science Center, Hiroshima University, Kagamiyama 1-3-1, Higashi-Hiroshima 739-8526, Japan*

¹² *Institute of Astronomy and National Astronomical Observatory, Bulgarian Academy of Sciences, 72 Tsarigradsko Shosse Blvd., 1784 Sofia, Bulgaria*

¹³ *Shanghai Astronomical Observatory, Chinese Academy of Sciences, 80 Nandan Road, Shanghai 200030, China*

¹⁴ *Crimean Astrophysical Observatory, P/O Nauchny, Crimea, 298409, Russia*

¹⁵ *Center for Astrophysics, Guangzhou University, Guangzhou 510006, China*

¹⁶ *Department of Physics, Tokyo Institute of Technology, 2-12-1 Ookayama, Meguro-ku, Tokyo 152-8551, Japan*

13 March 2022

ABSTRACT

We present a multi-wavelength spectral and temporal analysis of the blazar OJ 287 during its recent activity between December 2015 – May 2016, showing strong variability in the near-infrared (NIR) to X-ray energies with detection at γ -ray energies as well. Most of the optical flux variations exhibit strong changes in polarization angle and degree. All the inter-band time lags are consistent with simultaneous emissions. Interestingly, on days with excellent data coverage in the NIR–UV bands, the spectral energy distributions (SEDs) show signatures of bumps in the visible–UV bands, never seen before in this source. The optical bump can be explained as accretion-disk emission associated with the primary black hole of mass $\sim 1.8 \times 10^{10} M_{\odot}$ while the little bump feature in the optical–UV appears consistent with line emission. Further, the broadband SEDs extracted during the first flare and during a quiescent period during this span show very different γ -ray spectra compared to previously observed flare or quiescent spectra. The probable thermal bump in the visible seems to have been

clearly present since May 2013, as found by examining all available NIR-optical observations, and favors the binary super-massive black hole model. The simultaneous multi-wavelength variability and relatively weak γ -ray emission that shows a shift in the SED peak is consistent with γ -ray emission originating from inverse Compton scattering of photons from the line emission that apparently contributes to the little blue bump.

Key words: BL Lac objects: individual: OJ 287 – galaxies: active – – galaxies: jets – radiation mechanisms: non-thermal – X-rays: galaxies

1 INTRODUCTION

OJ 287 belongs to the BL Lacertae subclass of blazars, a class of radio-loud active galactic nuclei (AGN) with relativistic jets aligned at small angles to the observer’s line of sight and with very weak or no emission lines in their optical-ultraviolet spectra. The emission is almost entirely non-thermal, spanning the full observable electromagnetic spectrum, and is characterized by strong and rapid variability with high radio-to-optical polarization and frequent detections of superluminal features (Lister et al. 2013). Blazar variability is observed in all domains: temporal, spatial, spectral and polarimetric, and covers a wide range in each. In the time domain, the variability across the spectrum is erratic and stochastic, and is seen on all timescales from minutes to decades. The spectral domain, on the other hand, shows the characteristic broad double humped spectral energy distributions (SEDs) with a low energy hump peaking between infra-red (IR) and ultraviolet, or sometimes, soft X-ray bands, while the high energy hump reaches its maximum at γ -ray energies (Fossati et al. 1998; Mao et al. 2016). The emission at the low energy hump is understood to be the synchrotron emission from relativistic non-thermal electrons in the jet owing to the high degree of polarization in radio and optical bands, which often changes with the flux state of the source. The origin of the high energy emission, on the other hand, is less certain; while it probably results from inverse Compton (IC) processes, a hadronic origin is also plausible (e.g. Mücke & Protheroe 2001).

OJ 287 ($z = 0.306$) is one of the brightest and most highly variable BL Lac objects at radio and optical energies. It is also one of the most extensively observed extragalactic objects, with optical R-band data available since 1890. Despite blazars being known for stochastic temporal variations,

* E-mail: pankaj.kushwaha@iag.usp.br

† E-mail: acgupta30@gmail.com

‡ CAS PIFI Fellow

§ Email: wiitap@tcnj.edu

an extraordinary property of this source is the occurrence of ~ 12 year nearly periodic outbursts in its optical flux (Sillanpää et al. 1996a). Ever since this finding and its likely explanation in terms of a binary super-massive black hole (SMBH) system where the major flares are attributed to the secondary SMBH striking the accretion disc around the primary one (Sillanpää et al. 1988, but see Villforth et al. (2010)), it has been a prime target for multi-wavelength observations. OJ 287 has been monitored both intensively and extensively across the electromagnetic spectrum during the times of its expected outbursts (Valtonen & Sillanpää 2011; Valtonen et al. 2016; Gupta et al. 2017; Rakshit et al. 2017, and references therein). The early intensive observations revealed a double flare (Sillanpää et al. 1996b, see also Hudec et al. (2013)) and the SMBH binary model was refined and improved by incorporating inputs from these observations (Lehto & Valtonen 1996; Valtonen et al. 2006). These have led to attempts to predict and explain the emission properties (e.g. Pihajoki et al. 2013; Pihajoki 2016) and derive constraints on the system related to general relativistic effects such as loss of orbital energy through gravitational radiation (Valtonen et al. 2016). Apart from the ~ 12 y periodic feature, other periodic features have been claimed (Wu et al. 2006; Bhatta et al. 2016; Sandrinelli et al. 2016; Pihajoki, Valtonen, & Ciprini 2013). Although other models have been proposed, none of them have been as successful as the binary SMBH picture in term of predicting the occurrence of the flares at ~ 12 years periodicity (Valtonen, Ciprini, & Lehto 2012; Valtonen & Sillanpää 2011, and references therein); also see Villforth et al. (2010).

Apart from these photometric observations, the jet kinematics, multi-wavelength light curves, and polarization properties of OJ 287 have been studied in detail to understand the jet properties and the locations of flaring regions. Studies at radio energies using high resolution Very Large Baseline Array (VLBA) radio maps suggest a wobbling parsec-scale jet (Tateyama & Kingham 2004; Agudo et al. 2011; Moór et al. 2011) with changes in projected jet-position-angle of $> 100^\circ$ (Hodgson et al. 2017). In the optical, OJ 287 shows a preferred position angle in polarization, indicating the presence of both a steady core and a chaotic jet component (Villforth et al. 2010). On the other hand, correlation studies between γ -ray and radio emission show significant correlations with flaring episodes often associated with the ejection of superluminal components from stationary knots, located at parsec scales down the jet and seen in VLBA maps (Agudo et al. 2011; Sawada-Satoh et al. 2015; Hodgson et al. 2017). A similar location of a flaring region was inferred from the broadband SED modeling during a 2009 flare by Kushwaha, Sahayanathan, & Singh (2013).

Here, we present a correlation analysis of multi-wavelength (MW) observations of OJ 287 made before, during, and after its recent flaring in December 2015, which was predicted by the

binary SMBH model (Valtonen et al. 2011), and claimed to be the result of the impact of the secondary SMBH on the accretion disk of the primary. Valtonen et al. (2016) has already shown that the timing of this flare can provide a remarkably improved value of primary SMBH spin to 0.313 ± 0.01 , apart from producing values for the mass of the primary SMBH to be $(1.83 \pm 0.01) \times 10^{10} M_{\odot}$ and that of the secondary to be $(1.5 \pm 0.1) \times 10^8 M_{\odot}$, along with an orbital eccentricity of 0.700 ± 0.001 . Additionally, they also performed a preliminary modeling of the light curves and degree of polarization following Pihajoki (2016) and suggested that the X-ray emission is primarily non-thermal in origin. Intensive observations and intra-night variability during this period at optical energies have also been presented along with polarization data (Gupta et al. 2017; Rakshit et al. 2017). Our focus here is on what may be learned from MW emission and trying to understand the putative impact’s effect on MW emissions. We note that our observations extend through 2016 May, well beyond those discussed in Valtonen et al. (2016).

The paper is organized into five sections with §2 summarizing the MW data we have compiled and the procedures associated with them. The MW cross-correlation analyses and SEDs details and results are presented in §3. The implications of these results and a discussion is presented in §4, with our conclusions given in §5. A Λ CDM cosmology with $H_0 = 69.6 \text{ km s}^{-1} \text{ Mpc}^{-1}$, $\Omega_M = 0.286$ and $\Omega_{\Lambda} = 0.714$ is assumed for calculation of physical quantities.

2 MULTI-WAVELENGTH DATA AND REDUCTION

The MW data used here belongs both to publicly available data archives (X-ray, γ -ray, radio and a part of NIR-optical-UV measurements) as well as observations we made in the optical/NIR at specific observatories across the globe.

2.1 Fermi γ -ray Data

The γ -ray data belong to the *Fermi*-LAT (Large Area Telescope), an imaging telescope sensitive to photons with energies from 20 MeV to $> 300 \text{ GeV}$ (Atwood et al. 2009). Except for TOO observations, it is normally operated in all-sky scanning mode, covering the entire sky every ~ 3 hours. The LAT data being used here belong to one such normal operation mode from 15 October 2015 to 24 May 2016 (MJD: 57310 – 57560). The data were analyzed following the recommended procedures for the latest *PASS8* instrument response function data with the *Fermi Science Tool* version v10r0p5.

Our analysis considered only events between energies $0.1 \leq E \leq 300 \text{ GeV}$, categorized as “ev-

class=128, evtype=3” and within the maximum zenith angle of 90° from a circular region of interest (ROI) of 15° centered on the source. These events were further filtered with the appropriate good time intervals using the recommended criteria “(DATA_QUAL>0)&&(LAT_CONFIG==1)” to ensure that the instrument operation was in the normal scientific mode. The likely effects of these cuts and selections, as well as the presence of other sources in the ROI, were incorporated by generating an exposure map on the ROI and an additional annulus of 10° around it. We then modeled these events using ‘unbinned likelihood analysis’ with an input source model file from the 3rd LAT catalog (3FGL –gll_psc_v16.fit; [Acero et al. 2015](#)). The Galactic and isotropic extragalactic contributions were accounted for by using the respective templates, *gll_iem_v06.fits* and *iso_P8R2_SOURCE_V6_v06.txt* file provided by the instrument team. A significance criterion of 3σ , corresponding to a TS (Test Statistic) value of ~ 10 has been used for source detection.

We generated the daily γ -ray light curve following the above-mentioned procedures. The source was modeled with a log-parabola γ -ray spectrum while the default models, as used in the 3FGL catalog, were used for the rest of the sources in the input model file. For SEDs, the selected time intervals were further divided into logarithmic energy bins and a power-law model was used for each bin to extract the source flux. The γ -ray light curve is given in the top panel of Figure 1.

2.2 Swift X-ray and UV/Optical Data

X-ray: All the *Swift*-XRT observations taken during this period for OJ 287 were made in the photon counting (PC) pointed mode. Accordingly, the data files were first processed using the latest *CALDB* files via the *xrtpipeline* task with the default parameters. The events associated with the source and background regions, suitable for estimation of physical quantities of interest, were extracted using the *xselect* task with a circular source region of $47.2''$ (90% PSF, [Moretti et al. 2005](#)) and an annular region free of source contamination, respectively. None of the observations were found to have a count rate $\gtrsim 0.5$ counts/s, which would have required pile-up corrections. The effects of selections, cuts, and instrument operation related biases were estimated by generating an ancillary response file through the *xrtmkarf* task. Finally, we derived the flux assuming a power-law model with neutral hydrogen (nH) column density along the source direction fixed to the Galactic value of $2.38 \times 10^{20} \text{ cm}^{-2}$ using the corresponding ancillary files within *XSPEC*. The second panel of Figure 1 displays the *Swift* X-ray data reduced in this fashion.

UV/Optical: We have analyzed all the observations of the source OJ 287 performed by the *Swift* Ultraviolet and Optical Telescope (UVOT; [Roming et al. 2005](#)) between MJD 57354 and 557535.

In this study we have utilized only level 2 image mode data from UVOT in all filters (V, B, U, UVW1, UVM2, UVW2) in which the image is directly accumulated onboard, discarding the photon timing information so as to reduce the telemetry volume. We have used the standard procedure given on the *Swift* website¹ using the *uvotmaghist* task of the *heasoft* package for data reduction. *Swift*/UVOT source counts were extracted from a circular region of radius 5 arcsec, centred on the source position. The background counts were estimated from a nearby larger, source free, circular region of radius 20 arcsec. The source OJ 287 fluxes corresponding to the six optical/UV filters were corrected for Galactic reddening ($E(B-V) = 0.019$ mag; Schlegel, Finkbeiner, & Davis 1998). We have used equation (2) of Roming et al. (2009) to calculate the galactic extinction corrected flux of each spectral band. The third panel of Figure 1 shows the *Swift*/UVOT light curves.

2.3 Optical and Near-Infrared Data

Photometry: The bulk of the optical and near-infrared (NIR) photometric data we display here were taken at 11 observatories around the world in B, V, R, I, J and K bands, though the coverage is best in the R, B and V bands. The details of the telescopes from which we collected data in Bulgaria (3 telescopes), Chile (SMARTS²), Georgia, India, Japan, Serbia, and USA (2 telescopes), and how those data were reduced are presented in Gupta et al. (2017). We have now included photometric data from St. Petersburg University from the 70 cm telescope in Crimea and the 40 cm telescope in St. Petersburg Observatory, both equipped with nearly identical imaging photometers–polarimeters. The reduction of those observations is discussed in Larionov et al. (2008).

The photometric data were corrected for extinction following Schlafly & Finkbeiner (2011) with an $E(B-V)$ value of 0.0280 ± 0.0008 while the magnitude to flux conversion was performed using the zero point fluxes from Bessell, Castelli, & Plez (1998). These data are shown in the fourth through eighth rows of Figure 1. Although we do not display separate symbols for different observatories, one can see from Gupta et al. (2017) that whenever there are multiple measurements made at close times the agreements are excellent, and the same holds true for the new optical data that has been incorporated in this paper.

Polarimetry: We have obtained a substantial amount of polarimetric data from the St. Petersburg and Crimean telescopes. Polarimetric observations were performed using two Savart plates rotated by 45° relative to each another. By swapping the plates, the observer can obtain the relative

¹ <http://www.swift.ac.uk/analysis/uvot/>

² <http://www.astro.yale.edu/smarts/glast/tables/OJ287.tab>

Stokes q and u parameters from the two split images of each source in the field (Larionov et al. 2008). Instrumental polarization was found via stars located near the object under the assumption that their radiation is unpolarized. This is indicated also by the low level of extinction in the direction of OJ 287 ($A_V = 0.077$ mag; Schlafly & Finkbeiner 2011).

Additional polarimetric data for the same period have been taken from the public archive of the Steward Observatory of the University of Arizona. The details of this program and analysis procedures are discussed in Smith et al. (2009)³. These polarization data are presented in the second and third panels of Figure 2. We note that during periods of overlap the fractional polarization measurements agree extremely well, as do the polarization angles when the $\pm n\pi$ ambiguity is taken into consideration.

2.4 Radio data

Radio data at 15 GHz are taken from the public archive of Owens Valley Radio Observatory (OVRO). The observations were made using the 40 meter single dish radio telescope under the project *Monitoring of Fermi Blazars*⁴. The OVRO telescope monitors Fermi detected blazars north of 20° declination (Healey et al. 2008). The bottom panel of Figure 1 displays these radio data.

2.5 Multi-wavelength Light Curves

The resulting MW light curves are shown in Figure 1. Significant variability can be seen all across the electromagnetic spectrum with the optical-IR showing very prominent variations. The X-ray band is not very well sampled, but within the span of observations, it appears to reflect the changes seen in the optical-IR light curves, at least during the first half of the period. The γ -ray band also shows significant variations, but to the eye, they appear to be only roughly correlated with the optical-IR bands, while the sparsely sampled radio data show relatively smooth variations without any obvious connection to the other bands.

The polarization data show that there are at least two distinctly different types of flares coming from the source. The main flare at MJD 57361 which, according to the SMBH binary model, corresponds to the impact of the secondary on the primary's disk, evinces a relatively low polarization fraction ($PD \lesssim 11\%$), that differs little from that in the preceding quiescent period (see Fig. 3 in Valtonen et al. 2016). During its decay phase, the polarization angle (PA) undergoes a large swing

³ <http://james.as.arizona.edu/~psmith/Fermi>

⁴ <http://www.astro.caltech.edu/ovroblazars/>

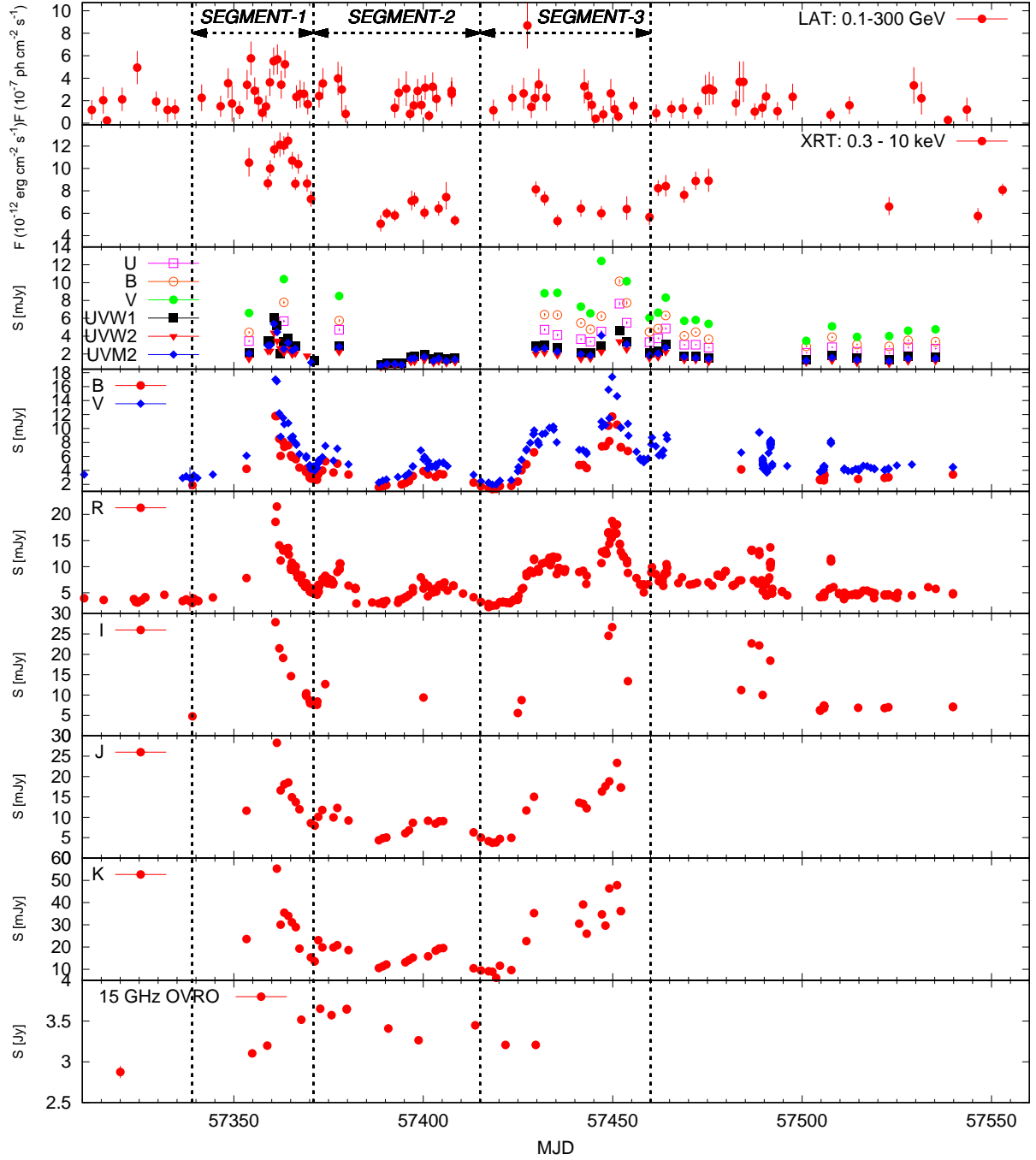


Figure 1. October 2015 – May 2016 multi-wavelength light curves of OJ 287 from γ -rays to radio. The vertical lines demarcate the sections considered for cross-correlation analyses in the present work.

of $\gtrsim 200^\circ$ while the PD varies quite a bit (Fig. 2), but other new flares appear soon thereafter. Almost all these flares until the second strong optical-NIR flare on MJD 57450 are associated with significant change in PA ($\gtrsim 90^\circ$) and PD both. We lack sufficient polarization coverage during the significant flare peaking at MJD 57378 but it is known to be highly polarized (30–40%; Fig. 3 of Valtonen et al. 2016). On the other hand, the flare around MJD 57400 is similar in its polarization properties to the strongest flare around MJD 57361, with a significant swing in PA, but only small

fluctuations around a modest value of PD. The subsequent flares at MJD 57435 and the very large one at MJD 57450 both show strong increments in PD, but the former corresponds to a slower swing in PA while the latter shows nothing detectable in that regard. We note that the flare at MJD 57435 does correspond to a single point excursion in the γ -ray flux. However, the strongest values of PD, exceeding 30%, are measured around MJD 57464 when the PA is nearly constant and only a small flare in overall flux is seen. The final significant flare in this period is at MJD 57490 and again the PD is low and variable, but the PA is essentially steady. It is certainly reasonable to take the flares with low PD to arise from predominantly thermal processes, while those with high PD may be associated with non-thermal, presumably jet-based, fluctuations (see also [Valtonen et al. 2016](#)).

3 SPECTRAL AND TEMPORAL VARIABILITY ANALYSIS AND RESULTS

To better understand the MW emission of OJ 287, we have performed cross-correlations between different bands and have examined the SEDs as a function of time. The former analysis contains imprints of particle acceleration and radiative cooling in different bands, while the latter helps us ascertain the nature of the emission processes and perhaps separate thermal from non-thermal emission components.

3.1 MW Cross-correlation Analysis

At the start of our observing campaign in September 2015, OJ 287 was in a low flux state. A strong outburst event started on November 14, 2015 which peaked on December 5, 2015 (MJD 57361). It is the first predicted outburst of the binary SMBH model [Valtonen et al. \(2011\)](#) and was detected and discussed by [Valtonen et al. \(2016\)](#). After this outburst until the end of our monitoring campaign, which lasted through May 2016, the blazar showed multiple flares at intervals averaging ~ 25 days. So the source is seen in several flare, pre-flare, and post-flare states over the course of eight months.

To look for lags between MW bands we performed a cross-correlation analysis using the *z-transformed discrete correlation function* (ZDCF) method ([Alexander 1997, 2013](#)) which works with both regularly and irregularly sampled data. In case of irregular sampling, the effects of non-uniformity and sparse sampling are accounted for by using equal population binning and Fisher's *z*-transform. Since by default, the method uses 11 data pairs per time bin, the duration for the correlation analysis chosen in this work is a compromise between the available number of data

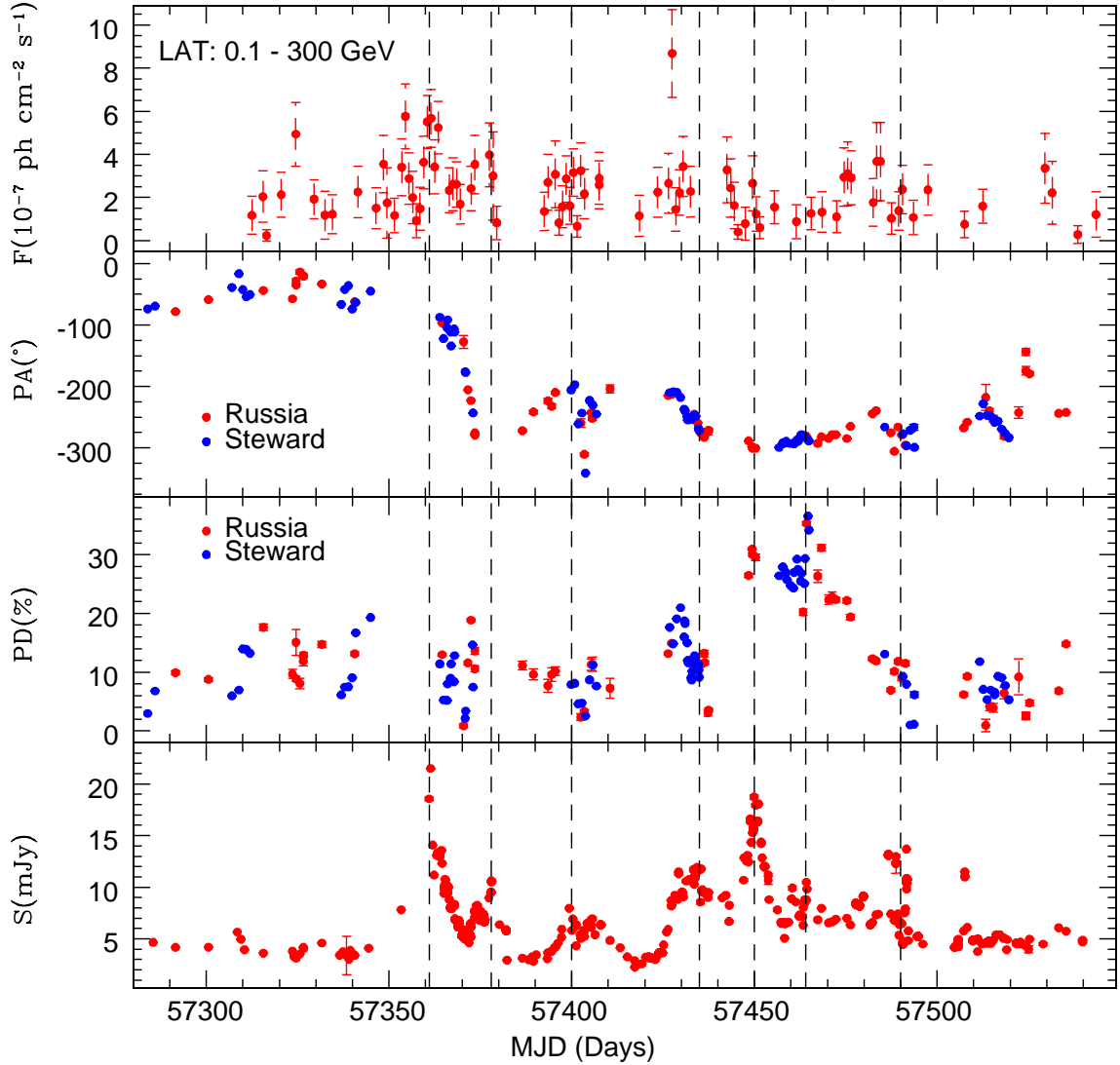


Figure 2. September 2015 – May 2016 optical polarization data plotted along with the γ -ray (top) and R-band (bottom) light curves of OJ 287. The dashed vertical lines note the peaks of the flares discussed in the text.

points and the different variability characteristics of OJ 287 across bands. To estimate the cross-correlation coefficients, the time lag bins are constructed by making all possible pairs of data points from one light curve with the data points of the other. These are then ordered based on the pairs' time differences. This ordered set is then binned, taking a minimum of 11 pairs per bin while discarding interdependent pairs from each bin. The newly formed bins correspond to a lag of the mean of the binned pairs (for more details see [Alexander 2013](#)). The coefficients are then calculated from these bins. For estimations of errors on the correlation coefficients, a Monte Carlo simulation of the light curve is performed using information about the observational errors on the

Table 1. Lag results for all the segments (in days)

Light curves	Segment-1 ¹	Segment-2 ²	Segment-3	Last Column, Fig. 3
γ vs V	+0.1 ^{+1.1} _{-2.2}	-1.2 ^{+1.7} _{-0.4}	—	-0.5 ^{+1.4} _{-6.0} (γ vs XRT) ¹
γ vs R	+1.2 ^{+0.9} _{-2.0}	+0.4 ^{+1.0} _{-1.2}	—	+0.16 ^{+1.6} _{-2.4} (XRT vs R) ¹
γ vs J	—	+5.0 ^{+4.7} _{-24.4}	—	+0.1 ^{+2.7} _{-2.7} (γ vs U1) ²
V vs R	+0.02 ^{+0.21} _{-0.12}	+0.23 ^{+0.28} _{-0.26}	0.0 ^{+0.9} _{-0.1}	+0.6 ^{+5.7} _{-3.4} (γ vs M2) ²
R vs J	—	+0.4 ^{+1.0} _{-1.0}	-0.06 ^{+0.27} _{-0.38}	-0.02 ^{+0.7} _{-0.6} (R vs U1) ²
J vs K	—	+0.2 ^{+3.7} _{-2.4}	+0.4 ^{+2.1} _{-2.1}	+0.01 ^{+0.67} _{-0.68} (R vs M2) ²

¹ for MJD 57339–57371 ² for MJD 57371–57425

fluxes. For each pair of simulated light curves, the correlation coefficients are estimated and then transformed to the z -space via (Alexander 1997, 2013)

$$z = \frac{1}{2} \ln \left(\frac{1+r}{1-r} \right), \quad \zeta = \frac{1}{2} \ln \left(\frac{1+\rho}{1-\rho} \right), \quad r = \tanh(z)$$

where r and ρ are, respectively, the bin correlation coefficient and the unknown population correlation coefficient. For ρ , it uses an ansatz $\rho = r$ to estimate the mean and variance of z (Alexander 2013, for more details). In the z -space, the transformed quantities are distributed normally. Thus, the error is estimated and finally transformed back to the correlation space providing 1σ errors on the coefficients.

The first three vertical sets of panels in Figure 3 show these correlations plotted as DCFs of: γ -ray vs optical (both V and R bands); γ -ray vs NIR (J); optical (V) vs optical (R); NIR (J) vs NIR (K); and optical (R) vs NIR (J). They were computed using the ZDCF method for three temporal segments chosen to illustrate different phases of the light curves: MJDs 57339–57371, 57371–57415, and 57415–57460, respectively denoted as Segments 1, 2, and 3 in Fig. 1. The fourth column of panels shows the DCFs between other bands for which we have enough measurements during some of these segments. The errors on the coefficients are derived from 1000 realizations of each light curve pair. The corresponding lag values are reported in Table 1 where a ‘—’ entry means not enough DCF points were available to derive lag values. A positive lag value between light curves in two different bands, labeled “ $LC1$ vs $LC2$ ” in Fig. 3 and Table 1 means that $LC2$ emission lags $LC1$, while a negative value would have $LC2$ leading $LC1$. We note that all nominal lags are within 1σ of 0.

3.2 Spectral Energy Distributions

In Figure 4, we show 72 daily NIR to UV SEDs taken between MJD 57350 (2015 November 24) and MJD 57485 (2016 April 7). Only dates for which we have observations in at least three different bands are plotted. Two striking features of these SEDs are the transition from a rather steep visible spectrum to a flatter one in the UV and the offset between the NIR and the vis-

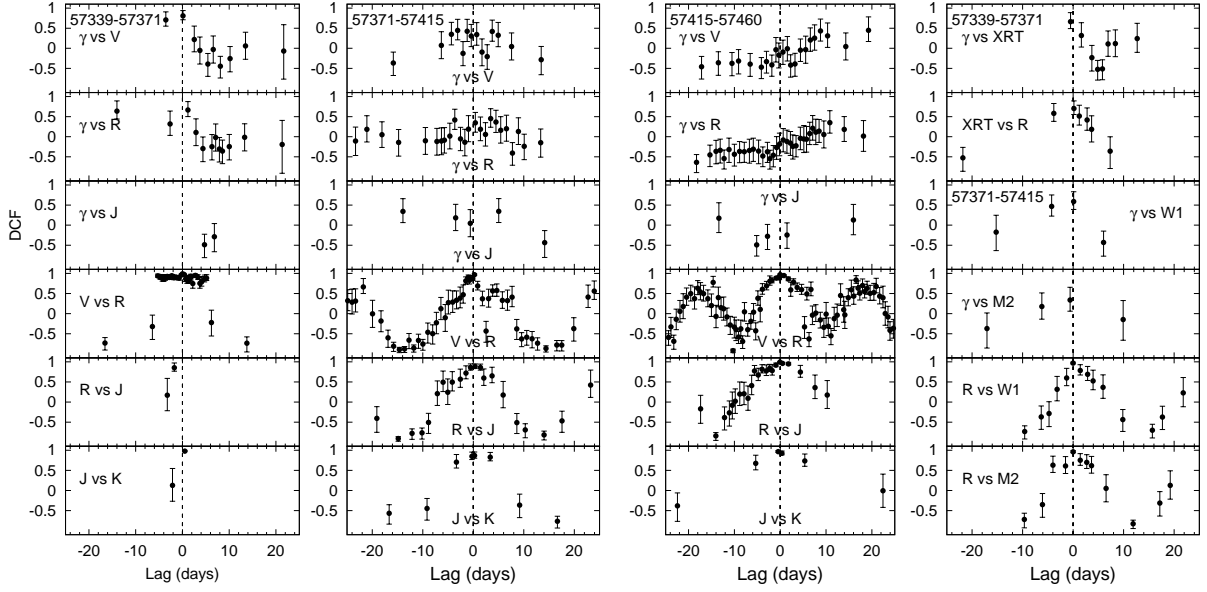


Figure 3. DCF of γ -ray vs optical (both V and R bands); γ -ray vs NIR (J); optical (V) vs optical (R); NIR (J) vs NIR (K); and optical (R) vs NIR (J) emission for the segments 1–3 defined by the dates in each panel of the near continuous multi-wavelength light curves of OJ 287 (see Figure 1). The vertical dashed lines correspond to zero lag between the light curves labeled as “LC1 vs LC2”. The last panel at right shows the DCF between other bands during these durations when data was informative (see §3.1).

ible portions. The overall broad enhancement in the optical/UV can be explained as the “big blue bump” arising from the multi-colour emission from the accretion disc (Sun & Malkan 1989; Raiteri et al. 2007) of the primary SMBH. The very high mass of the SMBH implies rather low accretion disc temperatures, and the modest redshift further lowers the peak wavelength of observed quasi-thermal emission (see SED modelling in §4). The additional flux in the visible causing the break between the optical and UV portions of the SED could correspond to a contribution from bremsstrahlung (Valtonen et al. 2016) with some flux arising from a “little blue bump” from emission lines (Raiteri et al. 2007; Gupta et al. 2017), though of course those are not strong in BL Lacs. The blue bump in the SED of OJ 287 does not appear to have been discussed previously and is hard to relate to jet activity (e.g. Valtonen, Ciprini, & Lehto 2012) and thus is a strong indication of a quasi-thermal, presumably, accretion disc, component. The modelling of the optical flare fluxes during the first portion of this light curve that was carried out by Valtonen et al. (2016) indicates the presence of an underlying component that is not obviously related to the jet and we may be detecting its spectrum through this filter photometry. While not uncommon in FSRQs (e.g. Raiteri et al. 2007; Ghisellini et al. 2017), to our knowledge, such a feature has not been seen previously in any BL Lac object.

In Figure 5, we present the NIR-optical SEDs from pre-major flare SMARTS measurements taken between MJD 56365 (2013 Mar 14) and MJD 57184 (2015 Jun 11). At the beginning of this period there is only a slight excess of the optical flux above the extrapolation of the NIR fluxes, but

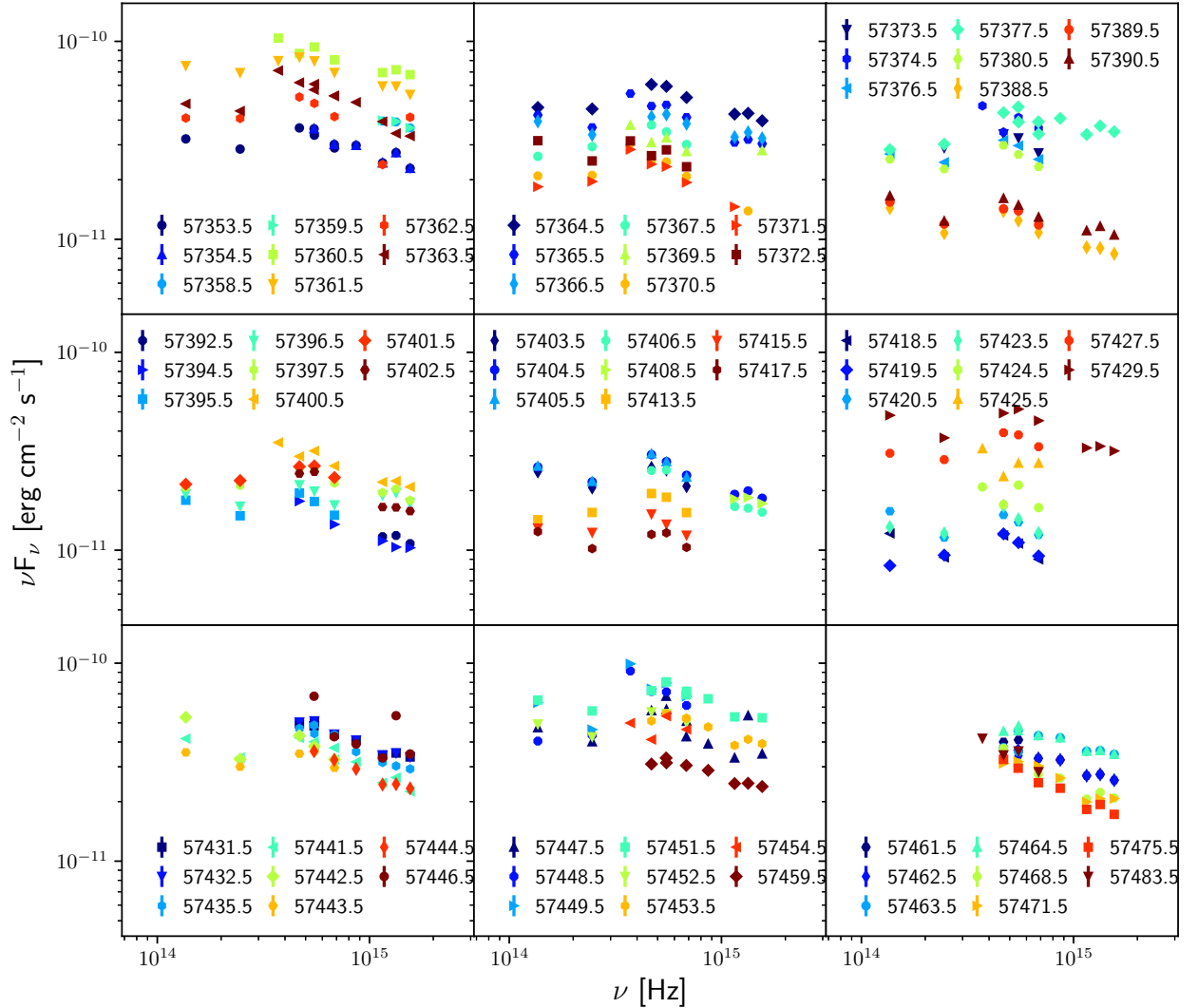


Figure 4. NIR to UV SEDs of OJ 287 between MJD 57350 – 57485 when the source was active and the sampling was good. Only dates having observations in at least 3 different bands are shown, labeled at the mid MJD.

starting on MJD 56439 (2013 May 27) there is a clear excess in the optical portion that presumably can be attributed to a substantial accretion disc contribution that we also saw during the November 2015 – April 2016 data presented in Figure 4.

In Figure 6, we present the MW broadband SEDs (see §4 for modelling) integrated over two different epochs: the flare (F) SED (MJD: 57359–57363) data were obtained when OJ 287 had simultaneous high fluxes in all the bands (excluding radio) and the quiescent (Q) SED (MJD: 57455–57469) that reflects a period when it was faint in the γ -rays and rather steady in the optical–UV bands. Interestingly, the γ -ray SEDs are very different from the previously published jet SEDs (e.g. Kushwaha, Sahayanathan, & Singh 2013; Seta et al. 2009) and show harder spectra with a clear shift in the location of the peak at γ -ray energies. Also, the optical polarization associated

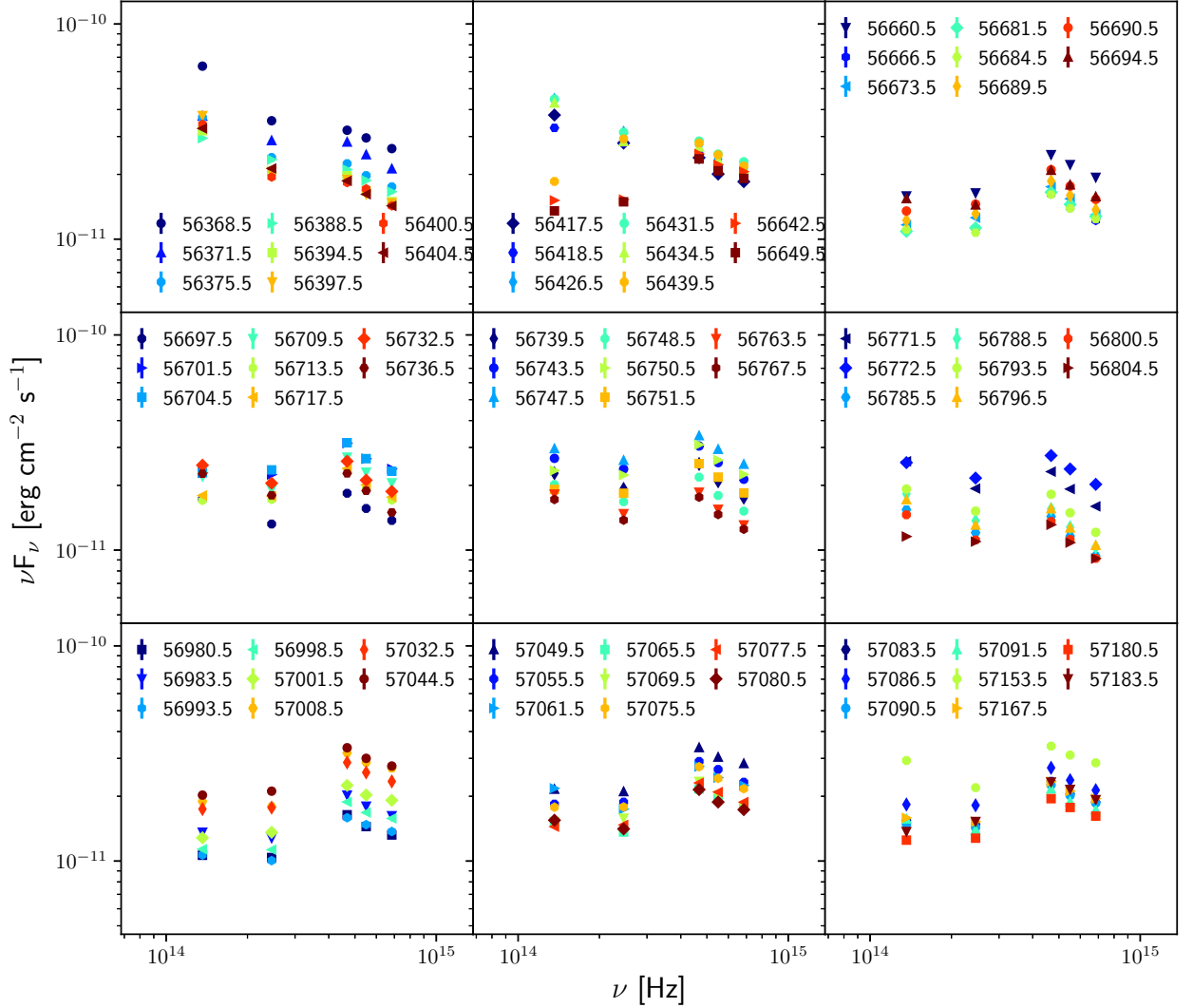


Figure 5. NIR to optical SEDs of OJ 287 between MJD 56365 – 57184, before the intensive multi-wavelength measurements of activity around December 2015 (labels as in Fig. 4).

with the first flare is low ($< 11\%$; Valtonen et al. 2016) compared to previous flares (Agudo et al. 2012) or some of the flares following that one (see Fig. 2) when significant rises are seen in optical bands.

4 DISCUSSION

We have performed a multi-wavelength correlation and spectral analysis of one of the high activity periods of OJ 287 in December 2015, which was predicted to occur (e.g. Valtonen & Sillanpää 2011), and is argued to be a result of the impact of a secondary SMBH on the primary’s accretion disk (Valtonen et al. 2016, and references therein; see more below). The multi-band correlation analyses were performed only for the periods when the data cadence available for both light curves

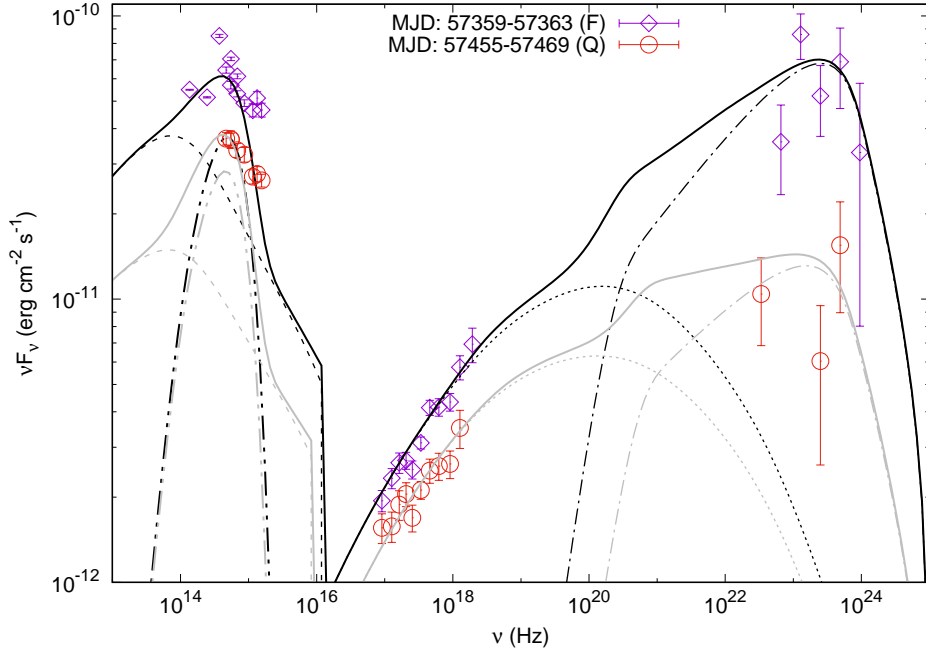


Figure 6. Broadband SEDs of OJ 287 during two different epochs corresponding to a flaring (F) and a quiescent state (Q) (see §3.2). For the model fits, the dashed, dotted, and dotted-dashed curves represent contributions from the synchrotron, SSC and IC of line emission (little blue bump in the UV), respectively, with black corresponding to the F state and grey to the Q. The double-dotted-dashed curves are the standard multi-temperature blackbody emissions from the accretion disc associated with the primary SMBH while the solid curves are the total emission (see §4).

were reasonably informative. However, the insufficiency of the sampling is clearly visible for several cross-band correlations (see Table 1). Despite this limitation, during temporal Segments 1 and 2 (MJD 57339–57415) when the data cadence is quite good, the results in Fig. 3 suggest that the variations between the NIR and γ -ray bands are simultaneous within the observational cadence. However, this is not the case for the γ -V/R/J correlations during the Segment 3 (MJD 57415–57460). The delays/lags suggested for that period by Fig. 3 are ambiguous, as while variations are seen in both γ -ray and optical–NIR bands, the light curves do not appear to be well correlated (Fig. 1). Further, the DCF values, even at the nominal delayed peaks in that segment, are rather low (DCF $\lesssim 0.5$) and hence are formally non-significant and thus, not quoted in Table 1. During Segment 3 there is a strong flare in the NIR–UV bands peaking at MJD 57450 that is nearly as powerful as the main flare in most of those bands, but it has no apparent X-ray or γ -ray counterpart and also has a much higher optical polarization than does the first flare, indicating a significant difference in its origin. In between these two strong NIR–optical flares (peak MJDs: 57365 and 57450), there are several other flares and almost all are associated with a significant change in PA ($\gtrsim 90^\circ$) and PD, indicating the presence of organized magnetic fields.

In the spectral domain, the detailed NIR–UV SEDs produced during the entire duration of the observations when sufficient data are available across these bands show clear signatures of

breaks between the NIR-visible and visible-UV spectra. The broad peak through the visible and UV part of the spectrum is good evidence for the presence of variable thermal accretion disc emission here making a significant contribution to the total flux although it is normally overwhelmed by the boosted jet emission in BL Lacs. In addition, the visible excess above the big blue bump may be attributed to bremsstrahlung (e.g. see [Valtonen & Wiik 2012](#); [Valtonen et al. 2016](#)), and perhaps, some emission from a weak broad line region. Further, the γ -ray portions of the two broad MW SEDs (see Fig. 6), are relatively flat (though quite noisy) and show a shift in the location of the peak of the SED at γ -rays, compared to the previously published SEDs ([Kushwaha, Sahayanathan, & Singh 2013](#); [Seta et al. 2009](#), see also [Valtonen, Ciprini, & Lehto \(2012\)](#)) for which the emission has been claimed to originate at parsec-scales down the jet ([Kushwaha, Sahayanathan, & Singh 2013](#); [Agudo et al. 2012](#)).

The first optical flare, peaking on MJD 57361 corresponds to the ~ 12 year near-periodicity discovered in the source over two decades ago. AGNs, in general, are believed to be comprised of several important constituents, including SMBH(s), accretion disc, corona, and, relativistic jets in the case of radio-loud sources, with possibly dynamically important magnetic fields. Hence, a quasi-periodicity can, in general, result from many processes in addition to the proposed binary SMBH model ([Lehto & Valtonen 1996](#)). One such process is jet precession, and it has been claimed in 3.5 cm radio observations of OJ 287 ([Tateyama & Kingham 2004](#)), but recent and better observations rather suggest a wobbling jet ([Agudo et al. 2012](#)). Other possible sources for the substantial variations on a decade-like timescale include a precessing disk and thus, jet (e.g. [Katz 1997](#)), perturbations in the inner part of the accretion disk (e.g. [Liu, Zhao, & Wu 2006](#); [Wang et al. 2014](#)), coherent helical motion of blobs in the jet ([Camenzind & Krockenberger 1992](#); [Mohan & Mangalam 2015](#)), and magnetic field related origins such as “magnetic breathing” ([Villforth et al. 2010](#), discussion and references therein). However, in a jet precession related origin, one expects similar light curve profiles in all bands and SEDs similar to those observed for the jet emission previously. Thus, although VLBA observations suggest the possibility of a precessing jet ([Tateyama & Kingham 2004](#); [Agudo et al. 2012](#)) at parsec-scales, the appearance of a likely thermal signature bump does not fit this picture well. Hence, we disfavor jet precession as the likely process for the ~ 12 years quasi-periodic variability, though it could be responsible for much longer time-scale variations as argued in [Valtonen & Wiik \(2012\)](#), see also [Villforth et al. \(2010\)](#)). Similarly, for a magnetic field dominated origin, the spectra are expected to be completely non-thermal in nature.

A low PD in the case of jet/magnetic origin of the flare can result from the presence of sub-

stantial turbulence in the emission region, but in such a case, a systematic rotation of PA is not expected (e.g. [Marscher 2014](#)). Another possibility for producing low PD is contamination from the putative jet from the secondary SMBH, if its polarization is opposite to that of the primary SMBH jet. This scenario can probably lead to large PA swing as well. However, this, as well as other possible signatures of binary nature of the source on polarization during the period of interaction, can be explored only with time-dependent modelling. It is important to note that the signature of the apparent thermal component is present throughout this period, from the occurrence of the first flare on 5 December 2015 through, as long as we had good NIR-optical-UV coverage. In fact, a detailed examination of the available SMARTS NIR-optical data shows that the bump in the NIR-visible part appeared first on MJD 56439 (2013 May 27) and appears to have been present since then (Fig. 5). Additionally, this thermal signature is seen in the bands where it is expected in the case of accretion disc around an SMBH of mass $\sim 1.8 \times 10^{10} M_{\odot}$, at the redshift of OJ 287, thereby further supporting the SMBH binary model for OJ 287.

The apparent simultaneous variability across the entire accessible electromagnetic spectrum (with the exception of the radio, where long lags are expected) during the flare period and most of the rest of these observations suggest that the observed quasi-thermal and non-thermal emission are either co-spatial or within a light-day or so apart from the disk. As OJ 287 is a blazar, the non-thermal emission can be associated with the jet of the primary, or even the secondary, SMBH. The latter has been argued to be probably aligned with the spin axis of the primary SMBH, and hence, should also have its putative jet pointed close toward us ([Valtonen et al. 2016](#)). On the other hand, the inferred simultaneous variability and the hard γ -ray spectra compared to those measured previously (e.g. [Kushwaha, Sahayanathan, & Singh 2013](#)), along with a shift in the SED peak, favors a leptonic origin of the second SED bump emission, with γ -rays resulting from IC of emission line photons, i.e., the little blue bump (optical-UV) that was never seen in previous studies.

As shown in Fig. 6, modelling of SEDs with a one-zone model, assuming synchrotron and IC scattering of both synchrotron and little blue bump photons from a broken power-law particle distribution, can successfully reproduce the observed broadband SEDs at the two epochs (e.g. see [Kushwaha, Sahayanathan, & Singh 2013](#), for more details on the modelling approach). In such one-zone models, the optically thin synchrotron (NIR-optical) and SSC (X-ray spectrum, away from the peak of the SED) emissions reflect the instantaneous particle spectrum. Thus the particle spectrum before the break is derived from the X-ray data, but due to thermal contamination at the NIR-optical part, we have used the quiescent state particle index from a previous study of

the OJ 287 by [Kushwaha, Sahayanathan, & Singh \(2013\)](#), whose approach we follow here. For an assumed particle spectrum, emission region size, and jet angle to the line of sight (θ), the flux due to IC of external field before the peak of the SED is (in a delta function approximation for the IC and synchrotron emission)

$$F(\nu_\gamma) \propto [\Gamma(1 + \cos\theta)]^{(p+1)/2} [\nu_\star \delta]^{(p+5)/2} K \nu_\gamma^{-(p-1)/2}, \quad (1)$$

where Γ , δ ($= [\Gamma(1 - \cos\theta)]^{-1}$), K , and ν_\star are respectively, the jet bulk Lorentz factor, Doppler factor, particle normalization, and the photon field for the IC scattering (little blue bump) with p and q (see below) being the indices before and after the break (γ_b) in the particle spectrum. Similarly, the synchrotron flux after the SED peak in the optical-NIR region is

$$F(\nu) \propto \delta^{(q+5)/2} B^{(p+1)/2} K \gamma_b^{(q-p)} \nu^{-(q-1)/2}, \quad (2)$$

where B is the magnetic field in the emission region and the SED peak of the synchrotron emission is related to Larmor frequency (ν_L) by

$$\nu_p^{syn} \approx \frac{\delta}{(1+z)} \gamma_b^2 \nu_L. \quad (3)$$

Thus, for a given δ , K can be estimated using Eqn. 1 for a given observed flux at a γ -ray energy while constraining γ_b by demanding the location of the SED peak below NIR K-band using Eqn. 3. With this, the magnetic field can be derived using Eqn. 2 such that the sum of synchrotron and thermal contribution reproduces the observed break at the NIR-optical part and the X-ray spectrum by SSC. We choose a δ value so that the system remains in equipartition⁵. The corresponding model parameters for the assumed particle spectrum are given in Table 2 where the size of the emission region has been kept the same for both flare and quiescent epochs. Due to the onset of the Klein-Nishina effect for the IC emission, the γ -ray spectra is essentially independent of the assumed NIR-optical particle spectrum. For the NIR-optical part of the SED, the non-thermal and thermal contributions are constrained so that the sum of those contributions does not exceed the observed data during the ‘‘F’’ state at NIR bands (K). However, for the ‘‘Q’’ state, due to lack of any data in NIR-bands then, we have simply scaled down the synchrotron part as well as the thermal part of the emission. The accretion-disk portion of the SED, on the other hand, is reproduced employing multi-temperature blackbody emission from the primary SMBH ($M \simeq 1.8 \times 10^{10} M_\odot$) assuming a 10% accretion efficiency. Our modelling suggests that the accretion rate is modestly temporally variable; however, one needs better constraints on the non-thermal contributions to more precisely estimate the accretion rates. Additionally, the simultaneous MW variability along with

⁵ particle energy density equals magnetic energy density

Table 2. SED parameters

Parameters	F	Q
Particle index before break (p) (from X-ray)	2.36	2.50
Particle index after break (q)	3.8	3.8
Magnetic field (Gauss)	0.9	1.1
particle break energy (γ_b^*)	1590	1721
Equipartition fraction**	1	1
Doppler factor	14	10
Jet power (erg/s)	3.0×10^{45}	2.3×10^{45}

Size of the emission region: 3×10^{16} cm

Jet angle to the line of sight: 3°

Minimum and maximum electron Lorentz factor: 40, 3×10^4

*in units of electron rest mass energy

** particle-energy-density/magnetic-energy-density

γ -rays arising from IC scattering of the little blue bump photons also constrain the location of the emission region to sub-parsec scales, i.e., within the line emission region, contrary to previous inferences of origin at parsec scales (Hodgson et al. 2017; Kushwaha, Sahayanathan, & Singh 2013; Agudo et al. 2012). Furthermore, for the given parameters, the IC of a putative 250 K blackbody field (Kushwaha, Sahayanathan, & Singh 2013) makes a negligible contribution. Bremsstrahlung, and/or an additional synchrotron component, being broadband emission, would not lead to the structure seen in the NIR, where the I-band excess is most likely the $H\alpha$ line-emission at the redshift of OJ 287, (e.g. Raiteri et al. (2007) for the J-band excess in 3C 454.3).

The near periodic occurrence of optical outbursts from OJ 287 every ~ 12 years and the associated multi-wavelength variability makes it an outstanding candidate for increasing our understanding of various aspects of disc-jet connections, other jet processes and various proposed models for them (e.g. Villforth et al. 2010, and discussion therein), even if it is an apparently unique case. Since the times of the flares can be predicted, observations can be scheduled for maximum possible coverage across the electromagnetic spectrum, which is much more difficult to do for normal blazars with their erratic fluctuations. The multi-wavelength variability data, including optical polarization information, presented here, along with that taken elsewhere for part of this flare (see Valtonen et al. 2016; Gupta et al. 2017), as well as for past and future outbursts, promise to answer some of the current issues related to understanding jets and accretion discs.

5 CONCLUSIONS

We performed a multi-wavelength spectral and temporal correlation analyses of emission from OJ 287 associated with its recent bright optical flaring activity observed in December 2015. The MW light curves from December 2015 – May 2016 show significant activity in all bands, most promi-

nently in NIR, optical, UV, and X-ray, with most of them associated with a significant change in PA and PD. The temporal variations are simultaneous in all these bands to within the observational cadences whenever there are sufficient data to properly estimate the lags.

In the spectral domain, several new features were observed in the NIR-UV and gamma-ray bands that have not been seen in previous studies of this source nor even in any other BL Lac source. Most importantly, the NIR-optical-UV SEDs show bumps in the NIR-optical and optical-UV with hints of excess in the I-band. The NIR-optical bump is consistent with a multi-temperature accretion disc emission from the primary SMBH of mass $\sim 1.8 \times 10^{10} M_{\odot}$, while the optical-UV bump seems consistent with line emission, probably a result of the observed heightened disc emission. Interestingly, the broadband SEDs extracted during a high activity state and a low activity state are also quite different from those of previously studied LAT-band SEDs at low and high states of OJ 287. Compared to previous SEDs, the present SEDs show hardening and a shift in the SED peak at γ -rays. The shift and a harder γ -ray spectrum are consistent with IC scattering of photons from the little-blue-bump, i.e., line-emission. This, along with the lack of any apparent lags between bands, suggest that the dominant emission region, at least during this period, is located at sub-parsec scales and so within the broad line region. The likely thermal bump in the visible/UV, which can be traced back to MJD 56439 using available NIR-optical data, coupled with the simultaneous multi-wavelength variability and relatively weak γ -ray emission seen during the period MJD 57310–57560 that we have focused upon here, favor the already well supported binary SMBH model.

ACKNOWLEDGEMENTS

The authors thank the referee Manasvita Joshi for valuable comments and suggestions. This research has made use of data, software and web tools of High Energy Astrophysics Science Archive Research Center (HEASARC), maintained by NASA’s Goddard Space Flight Center and up-to-date SMARTS optical/near-infrared light curves available at www.astro.yale.edu/smarts/glast/home.php. SMARTS observations of Large Area Telescope monitored blazars are supported by Yale University and Fermi GI grant NNX 12AP15G, and the SMARTS 1.3-m observing queue received support from NSF grant AST 0707627. Data from the Steward Observatory spectropolarimetric monitoring project were used. This programme is supported by Fermi Guest Investigator grants NNX08AW56G, NNX09AU10G, NNX12AO93G, and NNX15AU81G. The OVRO 40 m Telescope Fermi Blazar Monitoring Program is supported

by NASA under awards NNX08AW31G and NNX11A043G, and by the NSF under awards AST-0808050 and AST-1109911.

PK acknowledges support from FAPESP grant no. 2015/13933-0. ACG's work is partially supported by Chinese Academy of Sciences (CAS) President's International Fellowship Initiative (PIFI) grant no. 2016VMB073. PJW is grateful for hospitality at KIPAC, Stanford University, and SHAO during a sabbatical. HG is sponsored by a CAS Visiting Fellowship for Researchers from Developing Countries, CAS PIFI (grant no. 2014FFJB0005), supported by the NSFC Research Fund for International Young Scientists (grant no. 11450110398) and supported by a Special Financial Grant from the China Postdoctoral Science Foundation (grant no. 2016T90393). EMGDP acknowledges support from the Brazilian funding agencies FAPESP (grant 2013/10559-5) and CNPq (grant 306598/2009-4). The Abastumani team acknowledges financial support by the Shota Rustaveli National Science Foundation under contract FR/217950/16. The St. Petersburg University team acknowledges support from Russian RFBR grant 15-02-00949 and St. Petersburg University research grant 6.38.335.2015. GD and OV gratefully acknowledge the observing grant support from the Institute of Astronomy and Rozhen National Astronomical Observatory, Bulgaria Academy of Sciences, via bilateral joint research project "Observations of ICRF radio-sources visible in optical domain" (the head is GD). This work is a part of the Projects No. 176011 (Dynamics and kinematics of celestial bodies and systems), No 176004 (Stellar physics) and No 176021 (Visible and invisible matter in nearby galaxies: theory and observations) supported by the Ministry of Education, Science and Technological Development of the Republic of Serbia. The work of ES, AS, RB was partially supported by Scientific Research Fund of the Bulgarian Ministry of Education and Sciences under grant DN 08-1/2016. MFG is supported by the National Science Foundation of China (grants 11473054 and U1531245) and by the Science and Technology Commission of Shanghai Municipality (grant 14ZR1447100). ZZ is thankful for support from the CAS Hundred-Talented program (Y787081009). JHF's work is supported by the National Natural Science Foundation of China (NSFC U1531245) and Guangdong Innovation Team for Astrophysics (2014KCXTD014).

REFERENCES

- Acero F., et al., 2015, *ApJS*, 218, 23
Agarwal A., et al. 2015, *MNRAS*, 451, 3882
Agudo I., et al., 2011, *ApJ*, 726, L13
Agudo I., Marscher A. P., Jorstad S. G., Gómez J. L., Perucho M., Piner B. G., Rioja M., Dodson R., 2012, *ApJ*, 747, 63
Alexander T., 2013, arXiv:1302.1508

- Alexander T., 1997, *ASSL*, 218, 163
- Atwood W. B., et al., 2009, *ApJ*, 697, 1071
- Bessell M. S., Castelli F., Plez B., 1998, *A&A*, 333, 231
- Bhatta G., et al., 2016, *ApJ*, 832, 47
- Camenzind M., Krockenberger M., 1992, *A&A*, 255, 59
- Fossati G., Maraschi L., Celotti A., Comastri A., Ghisellini G., 1998, *MNRAS*, 299, 433
- Ghisellini G., Righi C., Costamante L., Tavecchio F., 2017, *MNRAS*, 469, 255
- Gupta A. C., et al., 2017, *MNRAS*, 465, 4423
- Healey S. E. et al., 2008, *ApJS*, 175, 97
- Hodgson J. A., et al., 2017, *A&A*, 597, A80
- Hudec R., Bašta M., Pihajoki P., Valtonen M., 2013, *A&A*, 559, A20
- Katz J. I., 1997, *ApJ*, 478, 527
- Kushwaha P., Sahayanathan S., Singh K. P., 2013, *MNRAS*, 433, 2380
- Kushwaha P., Singh K. P., Sahayanathan S., 2014, *ApJ*, 796, 61
- Larionov V. M., et al. 2008, *A&A*, 492, 389
- Lehto H. J., Valtonen M. J., 1996, *ApJ*, 460, 207
- Lister M. L., et al., 2013, *AJ*, 146, 120
- Liu F. K., Zhao G., Wu X.-B., 2006, *ApJ*, 650, 749
- Mannheim K., Biermann P. L., 1992, *A&A*, 253, L21
- Mao P., Urry C. M., Massaro F., Paggi A., Cauteruccio J., Künzel S. R., 2016, *ApJS*, 224, 26
- Marscher A. P., 2014, *ApJ*, 780, 87
- Meyer E. T., et al., 2017, arXiv:1701.05846
- Mohan P., Mangalam A., 2015, *ApJ*, 805, 91
- Moór A., Frey S., Lambert S. B., Titov O. A., Bakos J., 2011, *AJ*, 141, 178
- Moretti A., et al., 2005, *SPIE*, 5898, 360
- Mücke A., Protheroe R. J., 2001, *APH*, 15, 121
- Pihajoki P., 2016, *MNRAS*, 457, 1145
- Pihajoki P., et al., 2013, *ApJ*, 764, 5
- Pihajoki P., Valtonen M., Ciprini S., 2013, *MNRAS*, 434, 3122
- Potter W. J., Cotter G., 2013, *MNRAS*, 429, 1189
- Raiteri C. M. et al., 2007, *A&A*, 473, 819
- Rakshit S., Stalin C. S., Muneer S., Neha S., Paliya V. S., 2017, *ApJ*, 835, 275
- Roming P. W. A., et al., 2009, *ApJ*, 690, 163
- Roming P. W. A., et al., 2005, *SSRv*, 120, 95
- Sandrinelli A., Covino S., Dotti M., Treves A., 2016, *AJ*, 151, 54
- Sawada-Satoh S., et al., 2015, *PKAS*, 30, 429
- Schlafly E. F., Finkbeiner D. P., 2011, *ApJ*, 737, 103
- Schlegel D. J., Finkbeiner D. P., Davis M., 1998, *ApJ*, 500, 525
- Seta H., et al., 2009, *PASJ*, 61, 1011
- Sillanpää A., et al., 1996a, *A&A*, 305, L17
- Sillanpää A., et al., 1996b, *A&A*, 315, L13
- Sillanpää A., Haarala S., Valtonen M. J., Sundelius B., Byrd G. G., 1988, *ApJ*, 325, 628
- Smith P. S., Montiel E., Rightley S., Turner J., Schmidt G. D., Jannuzi B. T., 2009, 2009 Fermi Symposium, eConf Proc. C091122: arXiv:0912.3621
- Sun W.-H. & Malkan M. A. 1989, *ApJ*, 346, 68
- Tateyama C. E., 2013, *ApJS*, 205, 15

- Tateyama C. E., Kingham K. A., 2004, *ApJ*, 608, 149
- Valtonen M., Sillanpää A., 2011, *AcPol*, 51, 060000
- Valtonen M. J., Wiik K., 2012, *MNRAS*, 421, 1861
- Valtonen M. J., Ciprini S., Lehto H. J., 2012, *MNRAS*, 427, 77
- Valtonen M. J., et al., 2006, *ApJ*, 646, 36
- Valtonen M. J., Mikkola S., Lehto H. J., Gopakumar A., Hudec R., Polednikova J., 2011, *ApJ*, 742, 22
- Valtonen M. J., et al., 2016, *ApJ*, 819, L37
- Villforth C., et al., 2010, *MNRAS*, 402, 2087
- Wang J.-Y., An T., Baan W. A., Lu X.-L., 2014, *MNRAS*, 443, 58
- Wu J., et al., 2006, *AJ*, 132, 1256